XLIII CILAMCE
21-25, November, 2022
FOZ DO IGUAÇU – PR – BRAZIL

Nonlinear static and dynamic behavior of a multistable structure formed by elastically connected trusses

Carlos H. L. de Castro[1], Diego Orlando[2], Paulo B. Gonçalves[1]

[1]*Dept. of Civil and Environmental Engineering, Pontifical Catholic University of Rio de Janeiro – PUC-Rio*
Rua Marquês de São Vicente, 225, Gávea, 22451-900, Rio de Janeiro/RJ, Brazil
carlos.lima.castro@gmail.com, paulo@puc-rio.br
[2]*Dept. of Mechanics and Energy – FAT, State University of Rio de Janeiro – UERJ*
Rodovia Presidente Dutra, km 298, 27537-000, Resende, RJ, Brazil
dgorlando@gmail.com

Abstract. Multistable systems have proved to be important in several engineering areas, from nano to macrostructures. Important applications can be found in vibration control, deployable and collapsible structures, dynamic systems with a periodic pattern and in the development of new materials (metamaterials), among others. However, there is a need to investigate the static and dynamic behavior of these eminently non-linear systems. The most basic example of multistable structures is the classic Von Mises truss, which presents two configurations of stable equilibrium, that is, a bistable behavior. In this work, the multistable behavior of a sequence of Von Mises trusses connected through the insertion of a flexible element represented by a linear elastic spring is studied. This system has multiple equilibrium configurations, both stable and unstable, which significantly influences its non-linear static and dynamic behavior. For analysis, the nonlinear equilibrium and motion equations, in their dimensionless forms, are obtained through the criterion of minimum potential energy and Hamilton's principle. Their behavior is then investigated through the use of equipotential energy surfaces and curves, nonlinear equilibrium paths, phase planes and basins of attraction. The parametric analysis investigates the effect of the connection stiffness and the physical and geometric parameters of the trusses on the behavior of the system. Through the results, it is possible to observe the importance of geometric nonlinearity and connection stiffness in the dynamics and stability of this new class of structures.

Keywords: Multistability, Nonlinear Vibrations, Von Mises Trusses.

1 Introduction

Multistable systems have received increasing attention in recent years and have become an important research field in several engineering areas, from nano to macrostructures [1-12]. Traditionally, from a design point of view, instability phenomena have been considered as a limiting factor and should be avoided through appropriate design specifications, since it leads to loss of load carrying capacity and eventually damage and collapse of the structure. However, in recent years a paradigm shift has emerged where elastic instability can be used in a favorable way. Most applications have focused on multistable systems capable of assuming different equilibrium configurations. Recent applications include vibration control, deployable and collapsible structures, dynamic systems with a periodic pattern and in the development of new materials (metamaterials), among others. Therefore, there is a need to investigate the static and dynamic behavior of these eminently non-linear systems.

The classical example of this class of structures is the Von Mises truss, which the well-known bistable behavior can be used to build a structure with multiple configurations of stable equilibrium. Castro et al. [13] studied the static instability and the nonlinear free vibration of a multistable system formed by a sequence of Von Mises trusses connected by rigid bars, in this work, the rigid element is changed by a flexible one (a linear elastic spring), seeking to verify the influence of including the flexible element in the structural behavior already presented. This nonlinear model can be suitably used in systems that assume many stable configurations

throughout their useful life.

2 Problem formulation

The structural system investigated in this paper consists of a sequence of two Von Mises trusses linked by a flexible element (a linear elastic spring) in such a way that leads to a model with multiple equilibrium configurations, as illustrated in Fig. 1, where a represents the height of the upper truss, b the height of the lower truss, c half length of the symmetric truss base, K the stiffness of the linear elastic spring, k_1 the axial stiffness of upper truss, k_2 the axial stiffness of lower truss, v_1 the displacement of the upper truss central joint, v_2 the displacement of the lower truss central joint and P the static load applied at the top node.

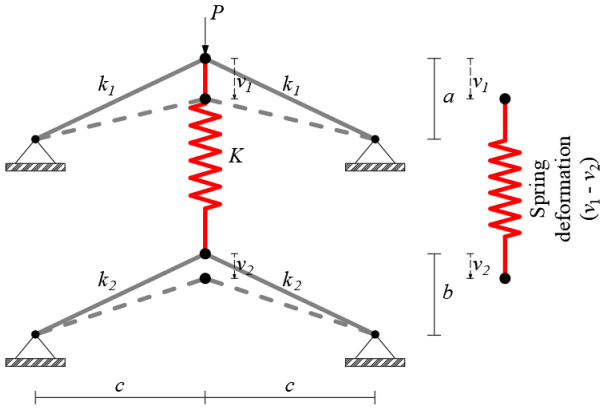

Figure 1. Model with two von Mises trusses coupled by a linear elastic spring.

The length of each truss bar before and after the application of the load P are given respectively by:

$$L1_i = \sqrt{a^2 + c^2},\ L2_i = \sqrt{b^2 + c^2} \text{ and } L1_f = \sqrt{(a - v_1)^2 + c^2},\ L2_f = \sqrt{(b - v_2)^2 + c^2}. \tag{1}$$

Considering the engineering strain (ε) and a linear, elastic material, the strain energy of each truss bar (Ub_i) and of the spring element (Us) are given by:

$$Ub_i = \int_0^{Li} \frac{1}{2} k_i (\varepsilon_i)^2 dx, \text{ where } \varepsilon_i = \frac{\Delta Li}{Li} = \frac{Li_f - Li_i}{Li_i},\ i = 1,2 \text{ and } Us = \frac{1}{2} K (v_1 - v_2)^2. \tag{2}$$

Collecting the contribution from trusses bars and the spring, the strain energy (U) and the gravitational potential energy of the applied load (V) are given respectively by:

$$U = \frac{1}{2} K (v_1 - v_2)^2 + k_1 L1_i \left(\frac{L1_f - L1_i}{L1_i} \right)^2 + k_2 L2_i \left(\frac{L2_f - L2_i}{L2_i} \right)^2 \text{ and } V = -P v_1. \tag{3}$$

So, the total potential energy of the system ($\Pi = U + V$) is:

$$\Pi = \frac{1}{2} K (v_1 - v_2)^2 + k_1 L1_i \left(\frac{L1_f - L1_i}{L1_i} \right)^2 + k_2 L2_i \left(\frac{L2_f - L2_i}{L2_i} \right)^2 - P v_1. \tag{4}$$

The kinetic energy is given by:

$$T = \frac{\rho A_0}{3} \left(\sqrt{a^2 + c^2}\, \dot{v}_1^{\,2} + \sqrt{b^2 + c^2}\, \dot{v}_2^{\,2} \right). \tag{5}$$

where the overdot represents the displacement derivative with respect to time t, ρ is material density and A_0 the undeformed cross section of the bars.

The following dimensionless parameters are adopted to conduct the parametric analysis:

$$a = \delta_1 c,\ b = \delta_2 c,\ k_2 = \alpha k_1,\ P = \lambda k_1,\ v_1 = \chi_1 a, v_2 = \chi_2 a,\ \tau = \omega_0 t,\ \kappa = \frac{Kc}{k_1},\ \omega_0^{\,2} = \frac{k_1}{\rho A_0 c^2},\ \bar{\Pi} = \frac{\Pi}{k_1 c} \text{ and } \bar{T} = \frac{T}{k_1 c}. \tag{6}$$

Then, the total potential energy and the kinetic energy can be rewritten in a dimensionless form as follows:

$$\overline{\Pi}=\frac{1}{2}\kappa\left(\chi_1\delta_1-\chi_2\delta_2\right)^2+\sqrt{\delta_1^{\,2}+1}\left(\frac{\sqrt{\left(\delta_1-\delta_1\chi_1\right)^2+1}}{\sqrt{\delta_1^{\,2}+1}}-1\right)^2+\alpha\sqrt{\delta_2^{\,2}+1}\left(\frac{\sqrt{\left(\delta_2-\delta_2\chi_2\right)^2+1}}{\sqrt{\delta_2^{\,2}+1}}-1\right)^2-\lambda\chi_1\delta_1. \tag{7}$$

$$\overline{T}=\frac{1}{3}\left(\delta_1^{\,2}\sqrt{\delta_1^{\,2}+1}\chi_{1,\tau}{}^2+\delta_2^{\,2}\sqrt{\delta_2^{\,2}+1}\chi_{2,\tau}{}^2\right). \tag{8}$$

Now, using the Langrage function ($\overline{L}=\overline{T}-\overline{\Pi}$) and the Hamilton's principle, the two nondimensional equations of motion takes the form:

$$\frac{2\delta_1\sqrt{\delta_1^{\,2}+1}}{3}\chi_{1,\tau\tau}+2\xi_1\delta_1\chi_{1,\tau}+\kappa(\chi_1\delta_1-\chi_2\delta_2)+\frac{2\left(\sqrt{\left(\delta_1-\chi_1\delta_1\right)^2+1}-\sqrt{\delta_1^{\,2}+1}\right)\left(-\delta_1+\chi_1\delta_1\right)}{\sqrt{\delta_1^{\,2}+1}\sqrt{\left(\delta_1-\chi_1\delta_1\right)^2+1}}-\lambda=\bar{Q}. \tag{9}$$

$$\frac{2\delta_2\sqrt{\delta_2^{\,2}+1}}{3}\chi_{2,\tau\tau}+2\xi_2\delta_2\chi_{2,\tau}-\kappa(\chi_1\delta_1-\chi_2\delta_2)+\frac{2\alpha\left(\sqrt{\left(\delta_2-\chi_2\delta_2\right)^2+1}-\sqrt{\delta_2^{\,2}+1}\right)\left(-\delta_2+\chi_2\delta_2\right)}{\sqrt{\delta_2^{\,2}+1}\sqrt{\left(\delta_2-\chi_2\delta_2\right)^2+1}}=\bar{Q}. \tag{10}$$

where $\bar{Q}=Q/k_1$ and ξ_1 and ξ_2 are the damping ratios.

3 Static analysis

3.1 Stability analysis

First, considering the minimum potential energy principle, the static behavior of the structure can be analyzed by the nonlinear equilibrium equations:

$$d\overline{\Pi}/d\chi_i=0,\quad i=1,2. \tag{11}$$

Choosing the dimensionless parameters α = 1.0, $\delta_1 = \delta_2$ = 0.14 and κ = 0.005, Fig. 2 presents the nonlinear equilibrium path with six limits points (blue dots). The nonlinear path displays four stable and three unstable branches separated by the limit points. The solid lines represent stable equilibrium states and dashed lines the unstable equilibrium states. While χ_1 increases and decreases under loading, exhibiting displacement limit points, χ_2 always increase. Under increasing load, the truss becomes unstable at $\lambda_{cr} = 1.32 \times 10^{-3}$ where the truss jumps to an equilibrium position were both trusses present an inverted equilibrium configuration. The results illustrate the complex nonlinear behavior of multistable systems and the energy gain or loss due to snap-through.

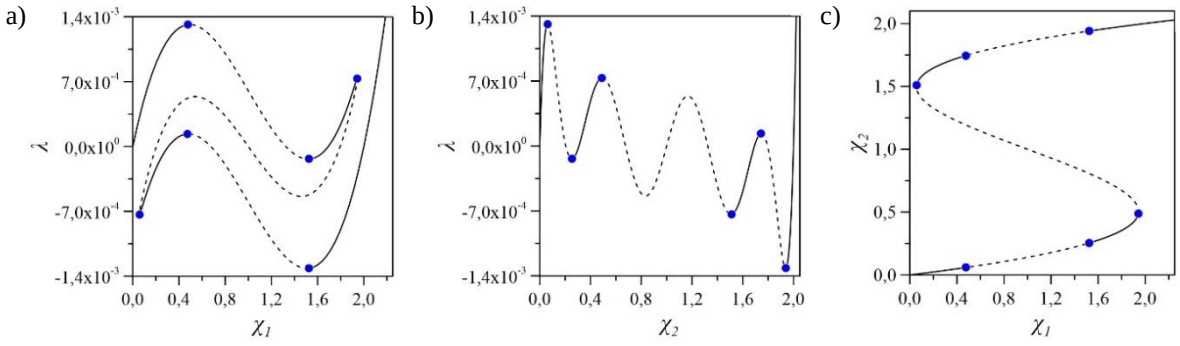

Figure 2. Nonlinear equilibrium path: a) $\lambda \times \chi_1$, b) $\lambda \times \chi_2$ and c) $\chi_1 \times \chi_2$

3.2 Variation of the potential energy

Figure 3 shown the total potential energy surfaces of the 2dof model for α = 1.0, $\delta_1 = \delta_2$ = 0.14,

$\kappa = 0.005$ and increasing static load levels. The multistable characteristic of the structural system is demonstrated by the presence of the four potential wells in Fig. 3(a). Three potential wells decrease with load and disappears at λ_{cr} while the potential well associated with the inverted position increases in depth. Saddles and maxima represent the unstable equilibrium configurations while the minima in each well represent the stable equilibria.

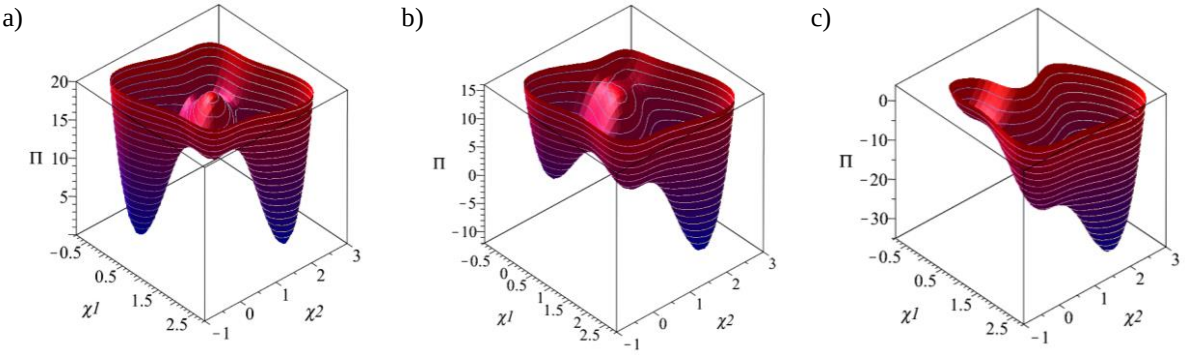

Figure 3. Potential energy variation (surface) with static load level: a) $\lambda = 0.0$ b) $\lambda = 4.0 \times 10^{-4}$ c) $\lambda = 12.0 \times 10^{-4}$

To better identify the equilibrium points, Fig. 4 present the equipotential energy curves for the same increasing static load levels used in Fig. 3. Red dots represent the maxima, blue, the minima, and black, the saddles. For the unloaded system (Fig. 4(a)), four stable equilibrium configurations of the structural system are observed: one pre-critical, (0,0), and three post-critical ((0.3,1.7), (1.7,0.3) and (2,2)). There is also the presence of the five unstable configurations: one maximum point, (1,1), and four saddles (0.2,1.3), (1.3,0.2), (0.7,1.8) and (1.8,0.7). The symmetries with respect to the two diagonals represent the inherent symmetries of the structural system. Figures 4(b) and 4(c) show the influence of the static load on the potential energy, decreasing the safe region associated with the pre-buckling equilibrium configuration, and, in a first moment, the disappearance of the region associated with the stable point (0.3,1.7), Fig. 4(b). Then, just before λ_{cr} the well associated with (1.7,0.3) also disappears as shown in Fig. 4(c).

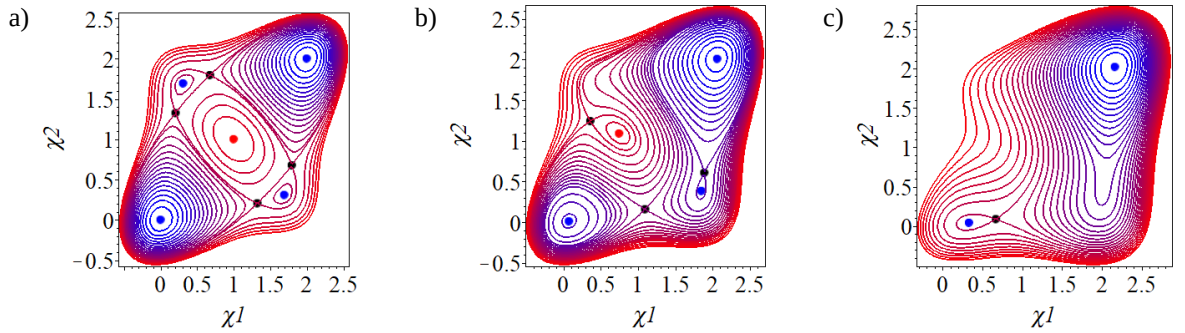

Figure 4. Variation of the curves of equipotential energy with the static load level: a) $\lambda = 0.0$ b) $\lambda = 4.0 \times 10^{-4}$ and c) $\lambda = 12.0 \times 10^{-4}$

4 Dynamic free vibration analysis

4.1 Natural frequencies

The natural frequencies and vibration modes are obtained by solving the associated eigenvalue problem. By expanding the nonlinear equations of motion in Taylor series, retaining the linear terms, and considering no damping and static load ($\xi_1 = \xi_2 = 0$ and $P = 0$), one obtains:

$$\left[[K]-\gamma[M]\right] X = 0 \quad \text{where} \quad \gamma = \bar{\omega}^2 \quad \text{and} \quad X = \{\chi_1 \quad \chi_2\}^T. \tag{12}$$

where K is the dimensionless stiffness matrix, M the dimensionless mass matrix and $\bar{\omega}$ is the natural frequency parameter.

Table 1 shows the results for some selected values of the dimensionless parameters (see Eq. 6). The lowest frequency corresponds to the in-phase vibration mode, while the second mode corresponds to the out-of-phase mode with the two trusses moving in opposite directions. The results clarify the influence of small variations in geometry (δ_1 and δ_2) and relative stiffness of the two trusses (α) and spring stiffness (κ) on the natural frequencies and second vibration mode.

Table 1. Natural frequencies and associated modes

α	δ_1	δ_2	κ	First ω	Eigenvector	Second ω	Eigenvector
1.0	0.10	0.10	0.005	0.1715	[1.0 1.0]	0.2105	[-1.000 1.000]
1.0	0.14	0.14	0.005	0.2379	[1.0 1.0]	0.2672	[-1.000 1.000]
1.0	0.10	0.10	0.006	0.1715	[1.0 1.0]	0.2175	[-1.000 1.000]
1.0	0.10	0.10	0.012	0.1715	[1.0 1.0]	0.2553	[-1.000 1.000]
1.0	0.10	0.12	0.005	0.1828	[1.0 1.0]	0.2300	[-0.558 2.582]
1.0	0.12	0.10	0.005	0.1828	[1.0 1.0]	0.2300	[-1.789 0.387]
0.8	0.10	0.10	0.005	0.1609	[1.0 1.0]	0.2049	[-1.469 0.681]
1.2	0.10	0.10	0.005	0.1783	[1.0 1.0]	0.2186	[-0.681 1.469]

Considering that the total displacement (χ_{nT}) as to the sum of static ($\chi_n i$) and dynamic ($\chi_n(t)$) displacements

$$\chi_{nT} = \chi_n(t) + \chi_n i. \tag{13}$$

it is possible to study the variation of fundamental frequency with the static load. Figure 5 shows the nonlinear frequency-load relation for different dimensionless parameters for selected values of $\delta_1 = \delta_2$ and for increasing levels of static load, where $\chi_n i$ is obtained from the nonlinear equilibrium path (Fig. 2).

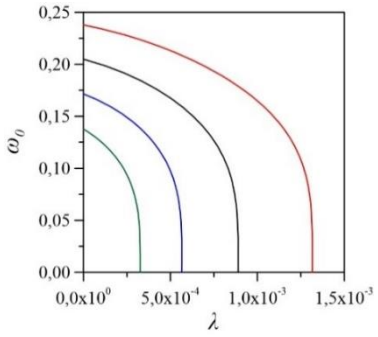

Figure 5. Variation of the fundamental frequency of the pre-buckling configuration with the static load level along the pre-buckling path for α = 1.0, κ = 0.00 and $\delta_1 = \delta_2$ = 0.08 (green), $\delta_1 = \delta_2$ = 0.10 (blue), $\delta_1 = \delta_2$ = 0.12 (black) and $\delta_1 = \delta_2$ = 0.14 (red).

4.2 Free vibration response

Considering a conservative system, from eq. (7) and (8), the conservation of energy principle leads to:

$$\bar{\Pi} + \bar{T} = C \tag{14}$$

where C is a given constant associated with the energy level obtained for a set of initial conditions and a given static load level.

A four-dimensional phase space (χ_1, $\chi_{1,\tau}$, χ_2 and $\chi_{2,\tau}$) is obtained by choosing a static equilibrium position. Figure 6 presents the four cross-sections of the four-dimensional phase space for different energy levels having as a reference the unloaded equilibrium position showing, in agreement with the previous analyses, five centers (four attractors and one repellor) and four saddles. The heteroclinic orbits connecting the saddles separate de different types of motion, including in-well and cross-well motions.

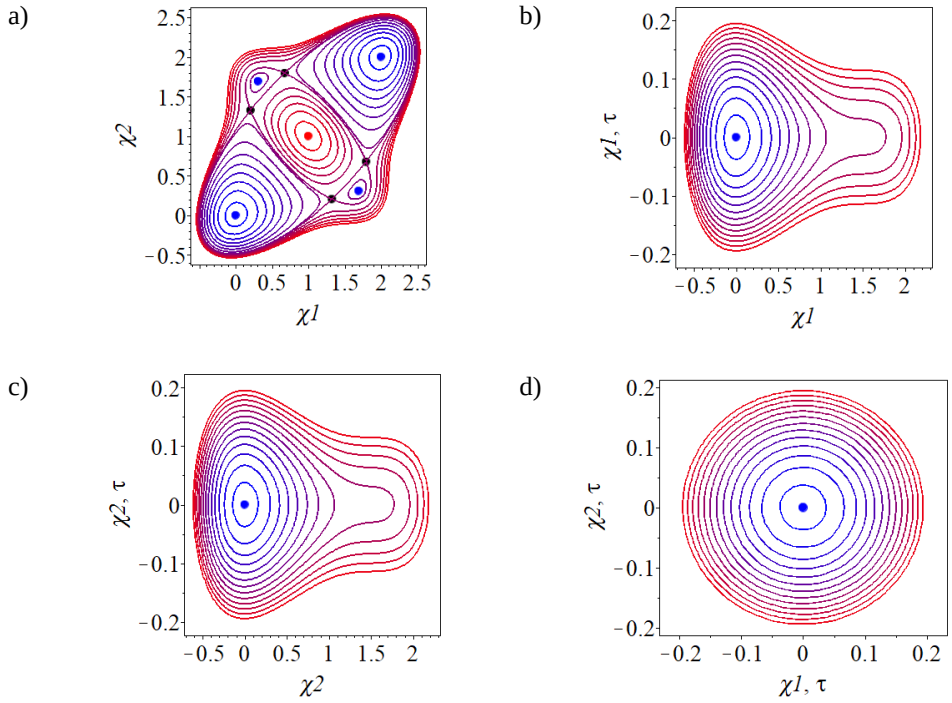

Figure 6. Isoenergetic curves of the unloaded system (λ = 0.0) for α = 1.0, κ = 0.005 and $\delta_1 = \delta_2$ = 0.14. a) $\chi_1 \times \chi_2$, b) $\chi_1 \times \chi_{1,\tau}$, c) $\chi_2 \times \chi_{2,\tau}$ and d) $\chi_{1,\tau} \times \chi_{2,\tau}$

But all systems have some dissipative effect and damping must be considered. So, for each set of initial conditions, the damped response will converge to one of the four coexisting attractors. Figure 7 shows sections the basins of attraction of the damped system in configuration space for increasing static load levels, λ. Saddles are represented by the yellow points and the attractors are marked by the white points in each region. Blue region denotes the pre-buckling basin of attraction while the black, red and green regions are the basins of attraction of the three post-buckling configurations. For λ = 0.0 the blue and green region are symmetrically distributed, the same occurring with the black and red ones. As λ increases, most initial conditions are connected to the green basin (the post-buckling equilibrium position where the two trusses are in an inverted position), while the blue region associated with pre-buckling equilibrium positions decreases considerably, evidencing the loss of dynamic integrity. Moreover, the red region is the first to disappear, followed by the black region, then by the blue region until only the green region remains for $\lambda > \lambda_{cr}$. Also the uncorrupted continuous basin around the attractor increases showing a growing robustness of the post-buckling equilibrium position under external disturbances.

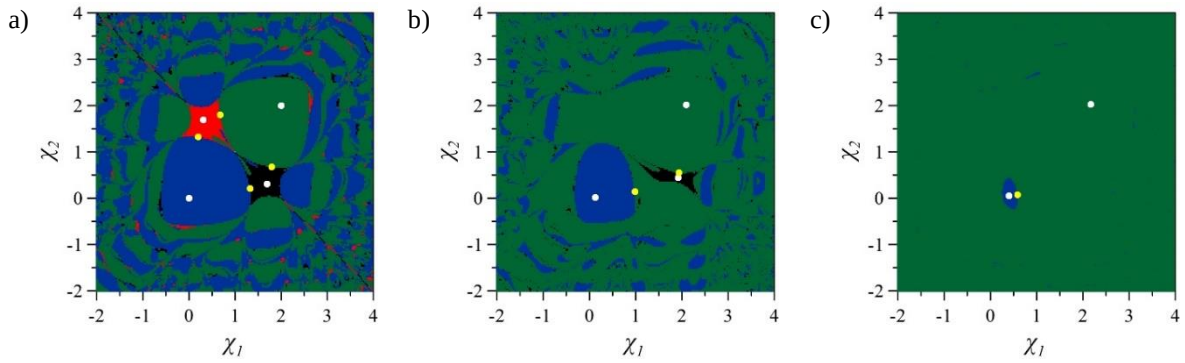

Figure 7. Basins of attraction for α = 1.0, κ = 0.005 and $\delta_1 = \delta_2$ = 0.14. a) λ = 0.0 b) $\lambda = 6.4 \times 10^{-4}$ and c) $\lambda = 12.8 \times 10^{-4}$. The attractor's coordinates are: a) (0.00, 0.00), (0.31, 1.69), (1.69, 0.31), (2.00, 2.00), b) (0.13, 0.02), (1.92, 0.44), (2.10, 2.01) and c) (0.40, 0.05), (2.17, 2.02).

5 Conclusions

The present work conducts an analysis of a structural system constituted by two shallow Von Mises trusses connected by a flexible element. The connection leads to a complex static multistable behavior. The unloaded structure displays nine equilibrium positions, four stable (attractors) and five unstable (four saddles and a repellors). Previous work [13] studied a similar model connected by rigid bars. Comparing both models, it is observed that the inclusion of a soft flexible element as a link between trusses leads to nonlinear equilibrium path with several limit points (load and displacement limit points) separating the stable and unstable equilibrium branches but no other bifurcation point. The effect of applied static load is analyzed using equipotential energy curves and basins of attraction. The results illustrate how an increasing static compressive load changes the size and depth of the four potential wells. They also show through evolution of the potential energy and basins of attraction the increasing sensitivity of the pre-buckling equilibrium configuration to external disturbances, demonstrating the loss of its dynamic integrity, whit phase-space dominated by the basin of the post-buckling equilibrium position where the two trusses are in an inverted position. Future work will include the nonlinear dynamic behavior of this model to assess its dynamic safety through bifurcation diagrams, basins of attraction and integrity measures [2, 11].

Acknowledgements. The authors acknowledge the financial support of the Brazilian research agencies CAPES, CNPq and FAPERJ.

Authorship statement. The authors hereby confirm that they are the sole liable persons responsible for the authorship of this work, and that all material that has been herein included as part of the present paper is either the property (and authorship) of the authors, or has the permission of the owners to be included here.

References

[1] Aza, C.; Pirrera, A.; Schenk, M. Multistable trusses of nonlinear morphing elements. In: *2018 International Conference on Reconfigurable Mechanisms and Robots (ReMAR)*. Delft, Holanda, 2018, p. 1-6.
[2] Benedetti, K. C. B.; Gonçalves, P. B.; Silva, F. M. A. Nonlinear oscillations and bifurcations of a multistable truss and dynamic integrity assessment via a Monte Carlo approach. *Meccanica*, v. 55, p. 2623–2657, 2020.
[3] Falope, F. O.; Pelliciari, M.; Lanzoni, L.; Tarantino, A. M. Snap-through and Eulerian buckling of the bi-stable von Mises truss in nonlinear elasticity: A theoretical, numerical and experimental investigation. *International Journal of Non-Linear Mechanics*. v. 134, p. 103739, 2021.
[4] Santana, M. V.; Arnouts, L. I. W.; Massart, T. J.; Gonçalves, P. B.; Berke, P. Z. Corotational 3D joint finite element tailored for the simulation of bistable deployable structures. *Engineering Structures*, v. 227, p. 111387, 2021.
[5] Cherston, J.; Strohmeier, P.; Paradiso, J. A. Grappler: Array of bistable elements for pinching net-like infrastructure to low gravity bodies. In: *AIAA Scitech 2019 Forum*. San Diego, California, 2019, p. 0871.
[6] Haddab, Y.; Aiche, G.; Hussein, H.; Salem, M. B.; Lutz, P.; Rubbert, L.; Renaud, P. Mechanical bistable structures for microrobotics and mesorobotics from microfabrication to additive manufacturing. In: *2018 International Conference on Manipulation, Automation and Robotics at Small Scales (MARSS)*. Nagoya, Japan, 2018, p. 1-6.
[7] Kidambi, N.; Zheng, Y.; Harne, R. L.; Wang, K. W. Energy release for the actuation and deployment of muscle-inspired asymmetrically multistable chains. In: *SPIE Smart Structures and Materials + Nondestructive Evaluation and Health Monitoring*. Denver, Colorado, USA. 2018, p. 1059510.
[8] Hua, J.; Lei, H.; Gao, C.; Guo, X.; Fang, D. Parameters analysis and optimization of a typical multistable mechanical metamaterial. *Extreme Mechanics Letters*. v. 35, p. 100640, 2020.
[9] Vincent, U. E.; Kenfack, A. Bifurcation and chaos in coupled periodically forced non-identical Duffing oscillators. *Chaotic Dynamics*, Jul. 2006. Available on: <https://arxiv.org/pdf/nlin/0607074.pdf> Access on: 22 may 2021.
[10] Santer, M.; Pellegrino, S. Compliant multistable structural elements. *International Journal of Solids and Structures*, v. 45, n. 24, p. 6190-6204, 2008.
[11] Orlando, D.; Castro, C. H. L. de; Gonçalves, P. B. Nonlinear vibrations and instability of a bistable shallow reticulated truss. *Nonlinear Dynamics*, v. 94, n. 2, p. 1479-1499, 2018.
[12] Fonseca, F. M., & Gonçalves, P. B. (2022). Nonlinear behavior and instabilities of a hyperelastic von Mises truss. *International Journal of Non-Linear Mechanics*, 142, 103964
[13] Castro C.H.L. de, Pantaleão R.J., Orlando D., Gonçalves P.B., Static and dynamic nonlinear behavior of a multistable structural system, *Proceedings of the joint CILAMCE-PANACM-2021*, Rio de Janeiro, Brazil, 2021